

Learning Knots Beyond Topological Invariants

Joseph Lahoud Sleiman,^{1,*} Filippo Conforto,^{1,*} Yair Augusto Gutierrez Fosado,¹ and Davide Michieletto^{1,2,†}

¹*School of Physics and Astronomy, University of Edinburgh,
Peter Guthrie Tait Road, Edinburgh, EH9 3FD, UK*

²*MRC Human Genetics Unit, Institute of Genetics and Cancer,
University of Edinburgh, Edinburgh EH4 2XU, UK*

ABSTRACT

Knots are deeply entangled with every branch of science. For more than a hundred years, the biggest open challenge in knot theory has been to formalise a knot invariant that can unambiguously distinguish any two knotted curves [1–3]. At the same time, the intuitive hypothesis that the geometry of a curve may encode information on the underlying curve topology remains an open conjecture [4]. Here, we propose a neural network (NN) approach that takes as input a geometric representation of a knotted curve and can classify knots more accurately than any existing knot polynomial. More specifically, we show that NNs trained using a “local writhe” representation can distinguish knots that share one or many topological invariants and knot polynomials, such as knot mutants. We also show that our approach can be scaled up to classify all knots up to 10-crossings with 95% accuracy. Our results not only pave the way to create artificial intelligence tools that can unambiguously classify and eventually generate curves with any knot topology but, perhaps more importantly, identifies local 3D writhe as a geometric signature of knot topology potentially leading to new topological invariants.

MAIN

Knots are fascinating objects that have captured the attention of humans for centuries. From Incas who used knotted Quipus to keep records [3] to Lord Kelvin who hypothesised elements were made of knotted ether [5] and to sailors and climbers whose lives often rely on some knotted rope. Knots are also deeply intertwined with history and art and often carry mystical meaning. The human obsession with knots brought Peter Guthrie Tait to compile the first knot tabulation of up to 10 crossings by hand [3]; currently more than one million unique knots up to 16 crossings have been tabulated using computer programs [6].

The rigorous proof that the early tabulated knots did not contain duplicates required the development of so-called topological invariants and knot polynomials, the

first of which was the Alexander polynomial [1], followed more recently by the Jones and HOMFLY polynomials [3, 7]. Knot polynomials are mathematical constructs that can be computed on knot diagrams and are invariant under smooth deformations of a curve, i.e. that preserve the curve topology. A famous exemplification of the power of knot polynomials came when two 10-crossings knots, erroneously classified as topologically distinct for 74 years, were found by Perko to in fact be the same knot [3]. In contrast to this, however, some knots share the same topological invariants and cannot be distinguished by these standard measures. Famously, the 11-crossing Conway knot has the same Alexander polynomial as the unknot and shares the same Jones polynomial of its mutant, the Kinoshita–Terasaka (KT) knot [8]. In fact, in general, all mutants of a knot have the same HOMFLY polynomials and the same hyperbolic volume [3].

Alongside the development of knot polynomials, several attempts were made to identify a relationship between a specific geometrical embedding of a knot and its underlying topology. This relationship differs from the one sought between so-called geometric and algebraic invariants [9, 10], e.g. the hyperbolic volume of a knot and its Jones polynomial. Perhaps the most famous result in this direction is the Fáry–Milnor theorem stating that the total absolute curvature of non-trivially knotted curves must be greater than 4π . This result only imposes a weak constrain on the topology of the underlying curve, as the unknot can itself have large curvature due to fluctuations of its contour. Likewise, Gauss proposed a formula to determine the number of times closed curves are linked with each other based only on the geometry of the curves [11]. A generalisation of the Gauss linking integral applied to a single closed curve is associated with its writhe [11] and average crossing number [12, 13]. Inspired by the intuition that writhe captures the level of geometrical entanglement of a curve with itself, we define a local segment-to-segment (StS) writhe generalisation

$$\omega_{StS}(x, y) = \frac{(\mathbf{t}(x) \times \mathbf{t}(y)) \cdot (\mathbf{r}(x) - \mathbf{r}(y))}{|\mathbf{r}(x) - \mathbf{r}(y)|^3}, \quad (1)$$

where $\mathbf{r}(x)$ and $\mathbf{t}(x)$ are the 3D position of, and the tangent at, segment x belonging to the closed curve γ , respectively. Intuitively, Eq. (1) captures the overall magnitude and the chirality of the entanglement between segment x and segment y (Fig. 1A-B). The quan-

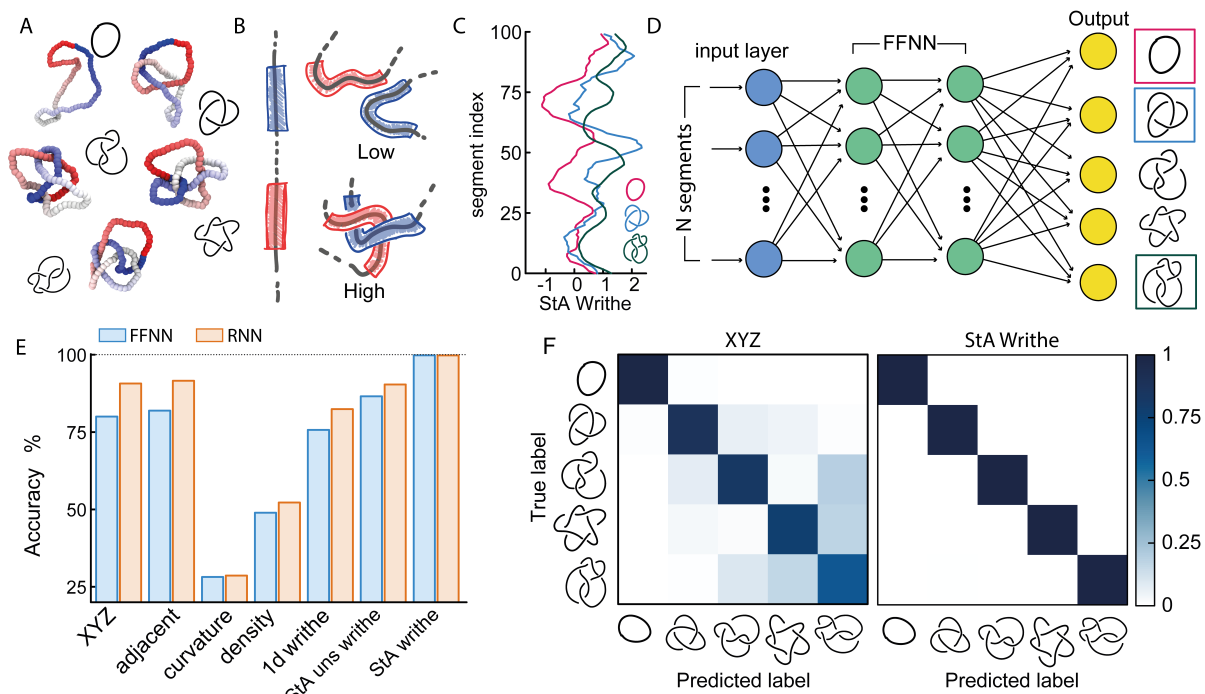


FIG. 1. **A** Examples of equilibrium knotted polymer conformations used as training set. We consider the 5 simplest knots: 0_1 , 3_1 , 4_1 , 5_1 and 5_2 . The colors follow the knot contour from red to white and then blue. **B** Graphical representation of StS writhe $\omega_{StS}(x, y)$. **C** Examples of patterns for $\omega_{StA}(x)$ for three different knots. **D** Graphical representation of the (feed-forward) network employed. The input layer contains N (or $3N$) neurons corresponding to the size of the input feature representation and the output layer yields a probability for each knot class. **E** Accuracy score, tested on unseen polymer conformations for different input features. The StA writhe classifies the 5-simplest knots with 99.9% accuracy. **F** Confusion matrices obtained by training the network with XYZ and StA writhe input features.

tity $\omega_{StA}(x) = \oint_{\gamma} \omega_{StS}(x, y) dy$ is the local segment-to-all (StA) writhe that characterises how geometrically entangled segment x is with respect to the rest of the curve.

The StA writhe, $\omega_{StA}(x)$, is a 1D geometrical representation of a knot that we hypothesise may display some features that are topology-dependent. Complex pattern recognition is a task that naturally lends itself to being addressed using a machine learning approach; we thus ask if a neural network trained at recognising patterns within $\omega_{StA}(x)$ is able to solve ambiguous knot classification problems. To do this we build feed forward and recurrent (long-short term memory, LSTM) neural networks (FFNN and RNN, respectively) and train them using $\sim 5 \cdot 10^5$ statistically uncorrelated and pre-labelled conformations of knotted bead-spring polymers which we simulated using LAMMPS [14]. To generate these configurations, we initialised a bead-spring polymer with known topology and $N = 100$ beads (unless otherwise stated) using KnotPlot (<https://knotplot.com/>), and subsequently evolved the polymer configurations via Langevin dynamics in an implicit solvent and fixed temperature using a Kremer-Grest model [15] to preserve polymer topology (see SI for more details). We confirmed that the topology was conserved either by computing their Alexander determinant via KymoKnot (<http://kymoknot.sissa.it>) [16] or, when ambiguous, visu-

ally.

The NNs are built with an input layer that was determined according to the representation being used; e.g., the Cartesian (XYZ) coordinate representation used 3 neurons (one for each dimension) per polymer bead. The other local input features used one neuron per bead, while the StS writhe feature requires $N \times N$ input neurons. The optimal number of hidden layers, hidden units, learning rate and batch size were determined via an automated hyperparameter tuning (*KerasTuner* [17]). Unless otherwise stated, our NNs contain 4 hidden layers, with around $4 \cdot 10^5$ trainable parameters. The output layer consists of C output neurons, corresponding to the C knot types being classified, each implemented with a softmax activation function in order to return the probability that a given input is a certain knot type. We took the sparse categorical cross-entropy as the loss function, as it was the most appropriate for individual class probabilities and integer target labels, i.e. our knot types (Fig. 1D).

We first tackle a 5-knot classification problem with the 5 simplest knots, which can be satisfactorily solved using NNs trained on center-of-mass-corrected Cartesian coordinates (XYZ) or adjacent bead input features [18, 19]. In line with these previous works, we find that our NNs can accurately predict the correct topology of around 80% of unseen conformations (80.1% with a FFNN and

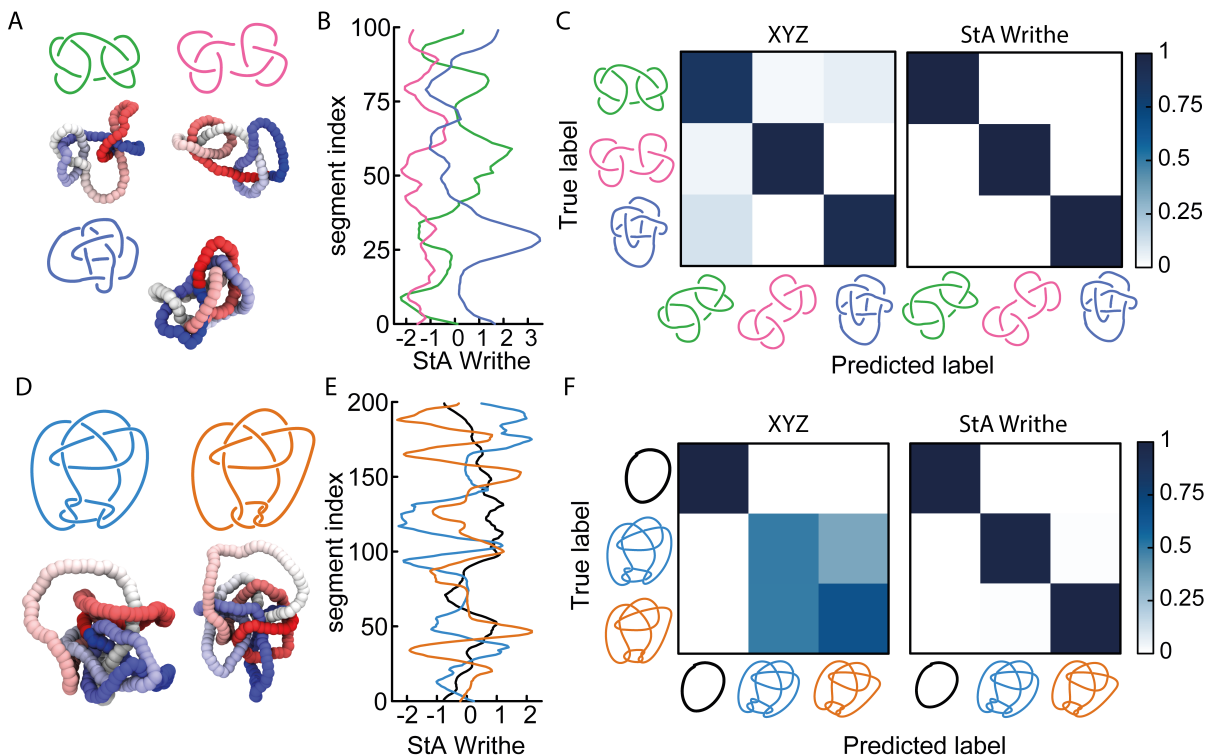


FIG. 2. **A** Snapshots of three knots with identical Alexander polynomial: square ($3_1^l \# 3_1^l$), granny ($3_1^l \# 3_1^l$) and 8_{20} knots. **B** Examples of StA writhe patterns from the three knots. **C** Confusion matrices obtained from a 3-class classification problem training a FFNN with XYZ (91.7% accuracy) or StA writhe (99.9% accuracy) features. **D** Snapshots of Conway (blue) and KT (orange) knots. **E** Examples of StA writhe patterns, including the one from the unknot (black). **F** Confusion matrices obtained from a 3-class classification problem training a FFNN with XYZ (67% accuracy) and StA writhe (99.5% accuracy).

86% with a recurrent NN architecture, Fig. 1E). These values are lower than the ones reported in Ref. [18] because we use a smaller training dataset. We then trained the same NNs using a range of other geometric features, such as local curvature, density and 1D writhe [20] (see SI for details), and found that most of them perform more poorly, or at best equally, with respect to the XYZ and adjacent representations (Fig. 1E). A similar outcome was obtained also in Ref. [19]. In striking contrast, models trained using $\omega_{StA}(x)$ outperform all other models and are found to achieve 99.9% accuracy, irrespectively if FFNN or RNN architectures (we also tested random forests, see SI). Additionally, the networks reached the early stopping criterion in about 50% fewer epochs than the ones trained by the XYZ representation. When plotted as a confusion matrix, the results clearly show that the XYZ input feature struggles to classify knots with a similar number of crossings, e.g. the 5_1 and 5_2 knots. On the contrary, our local 3d writhe feature generates a near-perfect confusion matrix (Fig. 1F).

Given that our NN approach can distinguish knots that share some knot invariants (e.g. the crossing number in the case of the 5-crossing knots), we now ask if our NN can also distinguish more complicated knots that share knot polynomials. To this end, we first consider three knots with identical Alexander polynomial, the

square, granny and 8_{20} knots (see Fig. 2A). The first two knots are composites of the trefoil with different chirality, and hence have 6 crossings, whereas the latter is an 8-crossings knot. Once again, we train a FFNN using the $\omega_{StA}(x)$ profiles (Fig. 2B) and obtain a striking accuracy of 99.98%, compared with 91.8% obtained by training with COM-shifted Cartesian coordinates (Fig. 2C). We then asked if our NN could also perform in situations where the knots shared multiple knot polynomials. As mentioned above, mutant knots share the same hyperbolic volume and several knot polynomials, including HOMFLY. We therefore performed simulations of the Conway (K11n34) knot and one of its mutants, the Kinoshita–Terasaka (KT, K11n42) knot. These 11-crossings knots have a number of identical knot invariants as they share the same Jones, Alexander and Conway polynomials [8]. Intriguingly, the latter two are also shared with the unknot. Thus, we generated 10^5 statistically uncorrelated conformations of 200-beads long polymers with the Conway, KT or unknot topologies (Fig. 2D) and trained our FFNN to classify these different topologies either using a COM-subtracted XYZ or $\omega_{StA}(x)$ (Fig. 2E) representations. When tested on unseen conformations we find that the NN trained with XYZ input features cannot distinguish between the Conway and KT knots, but both are accurately distinguished

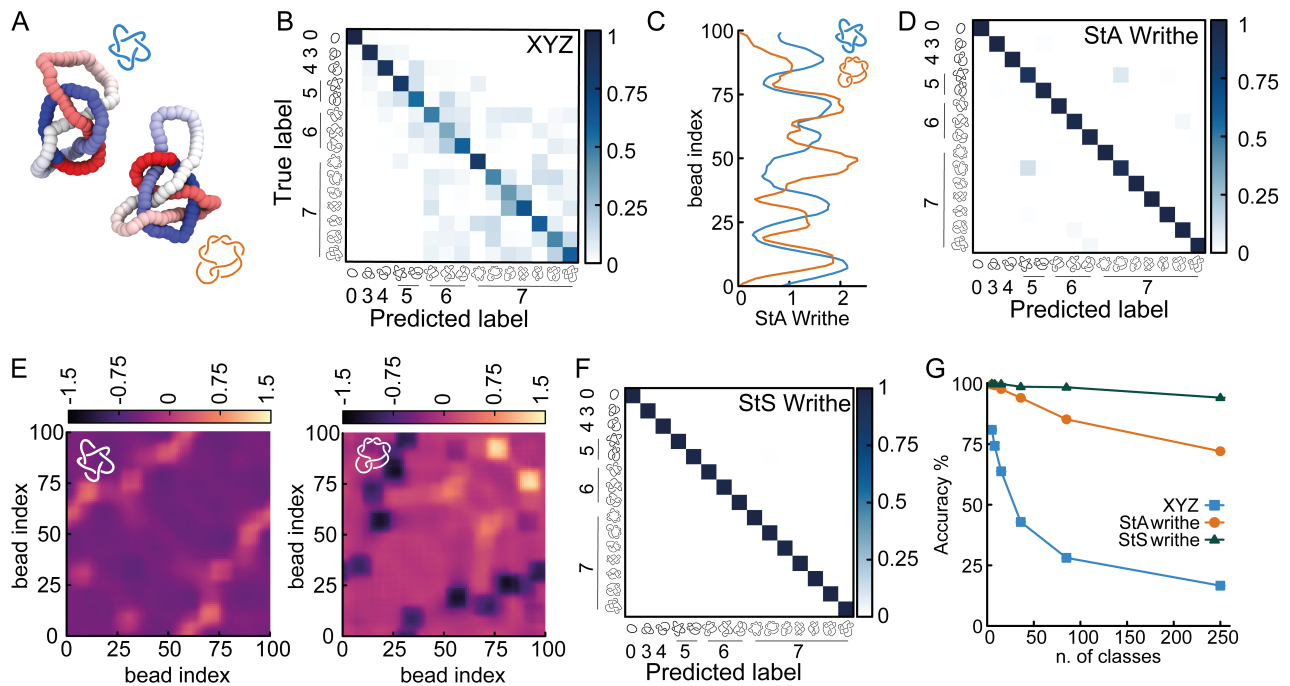


FIG. 3. **A** Two example conformations of 5_1 and 7_2 knots. **B** The XYZ-trained NN yields 63.8% accuracy and a rather sparse confusion matrix. **C** Examples of $\omega_{StA}(x)$ curves for the two knots, showing a degree of similarity between the pattern of maxima and minima. **D** The $\omega_{StA}(x)$ -trained NN achieves 98% accuracy and the confusion matrix shows that 5_1 and 7_2 are the knots that are most confused with each other. **E-F** Examples of $\omega_{StS}(x, y)$ geometric feature for the two knots corresponding to the $\omega_{StA}(x)$ profiles shown in **C**. **G** Accuracy for a 5-class classification problem with increasing average complexity of the knots being classified. **H** Accuracy as a function of number of knot classes to be distinguished.

from the unknot (Fig. 2F). On the other hand, we find that the NN trained with the local segment-to-all writhe once again perfectly disentangles the three knots with 99.6% accuracy (Fig. 2F). We therefore conclude that the NN trained with $\omega_{StA}(x)$ has the potential to unambiguously classify knots that share multiple knot polynomials, including knot mutants. In turn, we argue that this capability may be related to the fact that our $\omega_{StA}(x)$ -trained NN may contain a new topological invariant that outperforms existing knot polynomials.

To understand to which extent StA-trained NNs can be used to classify knotted curves, we decided to train our NN on an increasingly larger data sets, up to 10-crossings knots. Note that these 250 knots include 30 that share the same Alexander polynomial (see SI for a table), rendering them challenging to classify using standard tools such as Kymoknot. We first noticed that XYZ-trained NNs rapidly decreased accuracy when we included knots with 6 and more crossings (Fig. 3A-B). On the contrary, the CMs from StA-trained NNs remained more diagonal. In spite of this, we noticed that the knots 5_1 and 7_2 created some confusion also in the StA-trained NNs which dropped accuracy to 98% (Fig. 3C-D). We noticed that this was due to $\omega_{StA}(x)$ displaying similar patterns between the two knots (Fig. 3C). To further distinguish these (and potentially other knots with similar $\omega_{StA}(x)$ curves) we then considered our original proposition of lo-

cal StS writhe (Eq. (1)), reported in Fig. 3E, for the same 5_1 and 7_2 knots configurations used to compute $\omega_{StA}(x)$ in Fig. 3C. Interestingly, the $\omega_{StS}(x, y)$ heat maps appear very different, albeit when integrated along y and around the polymer contour, yield similar StA curves. We therefore trained our NNs using the StS writhe representation of the knots and re-established 99.8% accuracy (Fig. 3G). Ultimately, the NNs trained using the $\omega_{StS}(x, y)$ geometrical representation of knots yields the most accurate model, achieving 95% for a 250-class classification task including all knots up to 10 crossings. In comparison, the XYZ-trained and StA-trained NNs achieved 17% and 72%, respectively (Fig. 3G).

CONCLUSIONS

In conclusion, we have discovered that local 3d writhe (Eq. (1)) is a geometric descriptor of a curve that contains information about the underlying topology. We showed that NNs can access this information to classify the curve topology more accurately than they could do by using the Cartesian coordinates of the curve's segments (Fig. 1). We argue that NNs trained on local 3d writhe representation of knot conformations may numerically encode a new topological invariant that is more powerful than current ones. This conjecture is supported by the fact that even

a simple FFNN architecture can distinguish the topology of knot mutants that share several knot polynomials (Fig. 2). Our AI-driven approach can therefore classify complex topologies that would be otherwise impossible to disentangle using current tools. Finally, we show that our NN can naturally be turned into a tool to accurately classify a large number of random curves belonging to otherwise ambiguous knot topologies (Fig. 3). This approach naturally lends itself to be applied to protein folding [21], DNA [22, 23] and, in general, entanglements in complex systems [24–26].

METHODS

Knotted curves are modelled as semiflexible bead-spring polymers with $N = 100$ beads of size σ . The beads interact via a repulsive Lennard Jones potential, and are connected by FENE springs [15]. A bending rigidity is added via a Kratky-Porod potential. Each bead’s motion is then evolved via a Langevin equation with a friction and noise terms that obey the fluctuation-dissipation theorem. The numerical evolution of the Langevin equation is done with a velocity-Verlet scheme in LAMMPS [14]. The codes to generate these conformations are open access at <https://git.ecdf.ed.ac.uk/taplab/mlknotsproject>. We sample these simulations every 10^5 LAMMPS steps (or 10^4 Brownian times) to ensure that the conformations are statistically independent and uncorrelated (see SI for more details).

The NNS were built using TensorFlow [27] and the network hyperparameters were optimised using Keras-Tuner [17] using the XYZ representation (see SI for the values of hyperparameters used). We also implemented early stopping with a minimum of 0.001 accuracy improvement over 10 epochs. Datasets were randomly partitioned into training-validation-testing in a 90%/2.5%/7.5% whilst maintaining equal proportions of each knot type.

ACKNOWLEDGEMENTS

DM thanks the Royal Society for support through a University Research Fellowship. This project has received funding from the European Research Council (ERC) under the European Union’s Horizon 2020 research and innovation programme (grant agreement No 947918, TAP). JLS thanks the Physics of Life network for a student summer bursary in 2021 providing initial funds for this research. The authors thank Enzo Orlandini, Marco Baiesi, Pawel Dabrowski-Tumanski, Ken Millett, and Luigi del Debbio for insightful discussions.

- [1] J. W. Alexander, Transactions of the American Mathematical Society **30**, 275 (1928).
- [2] L. Kauffman, *Formal Knot Theory*, Mathematical Notes - Princeton University Press (Princeton University Press, 1983).
- [3] C. Adams, *The Knot Book* (W.H. Freeman, 1994).
- [4] J. Milnor, Annals of mathematics **52**, 248 (1950).
- [5] W. Thomson, Proceedings of the Royal Society of Edinburgh **6**, 95 (1867).
- [6] J. I. M. Hoste, M. Thistlethwaite, and J. Weeks, The Mathematical Intelligencer **20**, 33 (1998).
- [7] J. Hoste, Pacific Journal of Mathematics **124**, 295 (1986).
- [8] L. Piccirillo, Annals of Mathematics **191**, 581 (2020).
- [9] V. Jeyjala, A. Kar, and O. Parrikar, Physics Letters, Section B: Nuclear, Elementary Particle and High-Energy Physics **799**, 135033 (2019).
- [10] A. Davies, P. Veličković, L. Buesing, S. Blackwell, D. Zheng, N. Tomašev, R. Tanburn, P. Battaglia, C. Blundell, A. Juhász, M. Lackenby, G. Williamson, D. Hassabis, and P. Kohli, Nature **600**, 70 (2021).
- [11] M. R. Dennis and J. H. Hannay, Proc. R. Soc. A **461**, 3245 (2005).
- [12] A. Stasiak, V. Katritch, J. Bednar, D. Michoud, and J. Dubochet, Nature **384**, 122 (1996).
- [13] D. Michieletto, Soft Matter **12**, 9485 (2016).
- [14] S. Plimpton, J. Comp. Phys. **117**, 1 (1995).
- [15] K. Kremer and G. S. Grest, The Journal of Chemical Physics **92**, 5057 (1990).
- [16] L. Tubiana, G. Polles, E. Orlandini, and C. Micheletti, European Physical Journal E **41** (2018).
- [17] T. O’Malley, E. Bursztein, J. Long, F. Chollet, H. Jin, L. Invernizzi, *et al.*, “Keras Tuner,” <https://github.com/keras-team/keras-tuner> (2019).
- [18] O. Vandans, K. Yang, Z. Wu, and L. Dai, Physical Review E **101**, 1 (2020).
- [19] A. Braghetto, S. Kundu, M. Baiesi, and E. Orlandini, **56**, 2899–2909 (2022).
- [20] J. L. Sleiman, R. H. Burton, M. Caraglio, Y. A. Gutierrez Fosado, and D. Michieletto, ACS Polym. Au **2**, 341 (2022).
- [21] P. Dabrowski-Tumanski and J. I. Sulkowska, Proceedings of the National Academy of Sciences **114**, 3415 (2017).
- [22] J. T. Siebert, A. N. Kivel, L. P. Atkinson, T. J. Stevens, E. D. Laue, and P. Virnau, Polymers **9**, 1 (2017).
- [23] D. Goundaroulis, E. Lieberman Aiden, and A. Stasiak, Biophysical Journal **118**, 2268 (2020).
- [24] M. Dennis, R. King, B. Jack, K. O’Holleran, and M. Padgett, Nat. Phys. **6**, 118 (2010).
- [25] R. Everaers, Science **303**, 823 (2004).
- [26] F. Landuzzi, T. Nakamura, D. Michieletto, and T. Sakaue, , 5 (2020).
- [27] M. Abadi, A. Agarwal, P. Barham, E. Brevdo, Z. Chen, C. Citro, G. S. Corrado, A. Davis, J. Dean, M. Devin, S. Ghemawat, I. Goodfellow, A. Harp, G. Irving, M. Isard, Y. Jia, R. Jozefowicz, L. Kaiser, M. Kudlur, J. Levenberg, D. Mané, R. Monga, S. Moore, D. Murray, C. Olah, M. Schuster, J. Shlens, B. Steiner, I. Sutskever, K. Talwar, P. Tucker, V. Vanhoucke, V. Vasudevan, F. Viégas, O. Vinyals, P. Warden, M. Wattenberg, M. Wicke, Y. Yu, and X. Zheng, “TensorFlow: Large-scale machine learning on heterogeneous systems,” (2015), software available from tensorflow.org.

* joint first author

† corresponding author, davide.michieletto@ed.ac.uk